Enhancement of an Industrial Finite-Volume Code for Large-Eddy-Type Simulation of Incompressible High-Reynolds Number Flow Using Near-Wall Modelling

Tobias Knopp [a,*], Xiaoqin Zhang [b], Roland Kessler [a], Gert Lube [b]

[a] *Institut für Aerodynamik und Strömungstechnik, Deutsches Zentrum für Luft- und Raumfahrt, Bunsenstr. 10, D-37073 Göttingen, Germany*

[b] *Institut für Numerische und Angewandte Mathematik, Georg-August-Universität Göttingen, Lotzestrasse 16-18, D-37083 Göttingen, Germany*

Abstract

We present a validation strategy for enhancement of an unstructured industrial finite-volume solver designed for steady RANS problems for large eddy-type simulation with near-wall modelling of incompressible high-Reynolds number flow. Different parts of the projection-based discretisation are investigated to ensure LES capability of the numerical method. Turbulence model parameters are calibrated by using a minimisation of least-squares functionals for first and second order statistics of the basic benchmark problems decaying homogeneous turbulence and turbulent channel flow. Then the method is applied to the flow over a backward-facing step at $Re_h = 37500$. Of special interest is the role of the spatial and temporal discretisation error for low order schemes. For wall-bounded flows, present results confirm existing best practice guidelines for mesh design. For free shear layers, a sensor to quantify the resolution quality of the LES based on the resolved turbulent kinetic energy is presented and applied to the flow over a backward-facing step at $Re_h = 37500$.

Key words: Navier-Stokes model, large-eddy simulation, detached-eddy simulation, wall functions, projection method, finite volume method.

* Corresponding author.
Email address: Tobias.Knopp@dlr.de (Tobias Knopp).

1 Introduction

CFD has reached such a technology readiness level that it is used as standard predictive tool in a broad range of application areas. Virtually all of these tools rely on the (U)RANS approach which solves the statistically averaged (or: Reynolds averaged) Navier Stokes equations. Since RANS models are designed for problems with steady state solutions, the corresponding numerical methods traditionally use low order schemes. Here we restrict ourselves to incompressible flows, for which second order finite volume schemes are still very popular. The basic algorithms are well-established since more than two decades, see e.g. [13], and are still used by most research and commercial flow solvers. For a recent review see e.g. [12].
Comprehensive studies have shown that for certain classes of flows the (U)RANS modelling approach has become the limiting factor for getting high-quality numerical predictions. For most engineering simulations at design conditions, e.g., without (unsteady) flow separation, (U)RANS methods give predictions of satisfying accuracy. However, there is a strongly growing demand in predicting flows with incipient and moderate separation because industry requires more and more reliable predictions at the boundary of the operative range and for off-design conditions for airfoils, wind turbines, turbo-machinery etc.
The strong interest by research institutions and industry to use LES capabilities leads to the question whether existing RANS solvers or existing LES solvers should be used. Classical LES codes often provide higher order methods, but this restricts the applicability to simple geometries. Instead, RANS solvers are typically low order methods but often support unstructured meshes of hybrid element types and thus allow to deal with very complex geometries of industrial relevance easily. Several additional reasons lead to the aim to extend existing RANS solvers to LES capabilities. As RANS will be the backbone for industrial applications for the next future, the first application scenario will be to apply LES to carefully selected configurations after a broad simulation campaign using (U)RANS was performed. Moreover one has to keep in mind that development of a flow solver for complex industrial applications requires large costs for design, implementation, verification and validation until maturity is reached. Another important point is that it takes a long-term experience for engineers to become familiar with a CFD code and to acquire best-practice expertise until the code can be used as predictive tool, because there are always code-specific differences among different flow solvers. Moreover CFD has to be seen more and more as part of multiphysics applications, although a very important one. Such coupling of different codes and exchange of suitable data has been established for existing RANS solvers. Achieving LES capabilities while maintaining such interfaces is also of considerable interest.
When judging the industrial applicability of LES-type methods, one has to distinguish between two completely different groups. On the one hand, LES for complex configurations is naturally a grand challenge problem requiring

$\mathcal{O}(10^4)$ processors. On the other hand, industrial applicability of LES means that engineering design studies become feasible, meaning ultimately overnight LES simulations for configurations of moderate complexity. Currently the major part of industrial CFD applications is done by small and middle enterprises and engineering companies. Making LES amenable for clusters of $\mathcal{O}(10^1)$ processors used by this group should be a driving force regarding algorithmic development. For this purpose all simulations in this paper were performed on a single processor Linux machine. Acceleration techniques for LES are also of great interest for large scale applications because then the parameter space for design optimisation can be extended at the same total computing time.
Having pointed out the industrial need for LES and the reason to use existing RANS solvers, the question arises, whether it is possible to extend any second order RANS method to LES capability or not. Whereas (U)RANS solutions are characterized by smooth large-scale structures, turbulent flows have broad band spectra and the resolution of the medium to small eddies is crucial, see [23]. Thus the *first question* that arises is: *Is it possible to adopt second-order schemes in space and/or time for LES (or do we need higher order schemes)?* It is well-known that there are a variety of second order methods which allow for adequate LES simulations, e.g. the CDP-α code developed at Stanford university, see also e.g. [22]. The theoretical considerations by [9,14] have been recently reviewed by [27] with much more optimistic conclusions regarding the magnitude of numerical errors for second-order schemes. From this we conclude a positive answer for the first question. On the other hand it has to be mentioned that recent investigations clearly show significant advances of using sophisticated higher-order methods, see e.g. [5], which confirms earlier studies by [20,24].
The *second question* faces the huge computing costs: *Which (modelling) approaches are useful and applicable also to complex configurations to make LES amenable to high Reynolds number flows?* In this paper the focus is on wall-functions for alleviating the huge costs of wall-resolved LES by one order of magnitude, see e.g. [37,36]. As an alternative, the DES approach by [34] is also considered, which has been used as a wall-model for LES in [26]. It has become obvious that the coupling of a RANS type solution near the wall and an LES type solution for the outer flow requires special care, see e.g. [18]. This point will also be addressed in this paper.
The *third question* is: *How reliable are LES results in terms of numerical and modelling error?* This issue cannot be overestimated, in particular from an industrial point of view. Even when using RANS methods, CFD tools cannot produce results at the push of a button. Large user experience in choosing the correct numerical settings (grid design, parameters for the numerical solver) and turbulence modelling aspects is required. This is much more true for LES. The quality of the results strongly depends on the experience of the user. In the present work we focus on role of the discretisation error. For industrial applications of LES to flows in complex geometries, grid convergence cannot be reached or ensured by a global mesh refinement study due to extremely large

computational costs. For this reason we present a sensor based on the resolved turbulent kinetic energy which measures the resolution quality of the LES for free shear layers and in regions of separated flow. This sensor may then be used as a refinement indicator for local mesh adaptation. It is well known that also the sensitivity of the LES results to the inflow boundary conditions can be large, see e.g. [3,7,19], but this issue cannot be addressed here.
This *fourth question* is strongly related to the third one: *What are best-practice guidelines for LES?* Due to the extremely high computing costs, industry needs guidelines for mesh design, time step size and modelling aspects, see [33] as a very first step. Such guidelines should minimize erroneous computations and provide some general criteria for ensuring a proper use of LES in terms of numerical and modelling error. However, even for (U)RANS simulations, only first versions of best practice guidelines are available, e.g. [1].
In the present paper, we consider the unstructured incompressible finite volume solver THETA, developed at the German Aerospace Center (DLR) in Göttingen. At the start of this work, the THETA-code was validated only for laminar flows and for turbulent flows based on the RANS equations. For time accurate simulations only a first order accurate time discretisation scheme was available. Turbulence modelling was restricted to the standard k-ϵ model with classical wall functions.
The paper is organized as follows: In Section 2, we briefly describe the basic discretisation. Moreover, the models of LES and DES and aspects of the near-wall modelling will be introduced. Section 3 summarizes some tools to parameter identification problems for turbulent flows. The benchmark test case of decaying homogeneous turbulence is considered in Section 4. Turbulent channel flow is considered for Reynolds number $Re_\tau = 395$, see Section 5.1, and for higher Reynolds number $Re_\tau = 4800$ using wall-functions as near-wall model, see Section 5.2. In Section 6 the turbulent flow over a backward facing step at $Re_h = 37500$ is addressed and the sensor to measure the turbulence resolution is presented in Section 7. Summary and outlook are given in Section 8.

2 Basic discretisation and turbulence modelling

Consider the non-stationary, incompressible Navier-Stokes model

$$\partial_t \vec{u} - \vec{\nabla} \cdot (2\nu \mathbb{S}(\vec{u})) + \vec{\nabla} \cdot (\vec{u} \otimes \vec{u}) + \vec{\nabla} p = \vec{f} \qquad \text{in } \Omega \times (0,T] \qquad (1)$$

$$\vec{\nabla} \cdot \vec{u} = 0 \qquad \text{in } \Omega \times (0,T] \qquad (2)$$

for velocity $\vec{u}$ and pressure p in a bounded, polyhedral domain $\Omega \subset \mathbb{R}^3$ with given source term $\vec{f}$ and viscosity $\nu > 0$. $\mathbb{S}(\vec{u}) = \frac{1}{2}(\vec{\nabla}\vec{u} + \vec{\nabla}\vec{u}^T)$ is the rate of strain tensor. To simplify the presentation we set density to one. Appropriate boundary and initial conditions have to be added.
The spatial discretisation of (1)-(2) is based on a finite volume scheme on unstructured collocated grids. The primal and dual grids are sketched in Figure

1 (left). As the values of velocity and pressure are computed on the same set of nodes, the interpolation scheme by Rhie and Chow [30] is applied in order to avoid spurious pressure oscillations. Different upwind schemes (linear upwind scheme (LUDS), quadratic upwind scheme (QUDS)) and the central differencing scheme (CDS) are implemented for the approximation of the convective fluxes. Diffusive fluxes are discretized with CDS. The time discretisation is

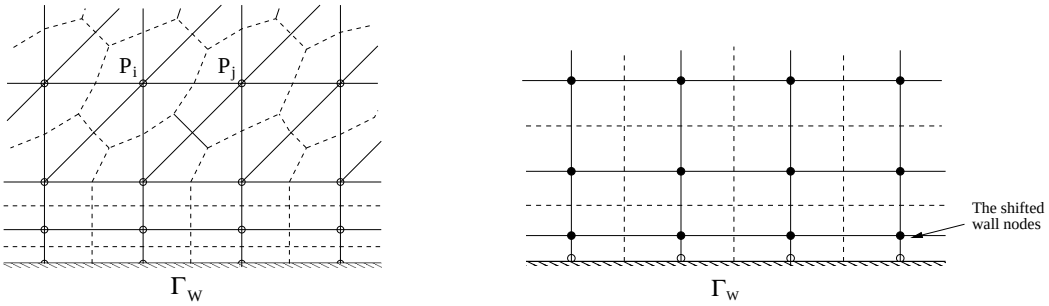

Fig. 1. Collocated grid arrangement: primal and dual grids (left), prismatic mesh in wall region (right)

performed using the A-stable BDF(2) scheme. The incremental variant of the projection method is used to split the calculation of velocity and pressure. Within each time step, the method is written as follows:

$$\frac{3\vec{u}^* - 4\vec{u}^n + \vec{u}^{n-1}}{2\delta t_n} + \vec{\nabla}\cdot(\vec{u}^*\otimes\vec{u}^*) - \vec{\nabla}\cdot(2\nu\mathbb{S}(\vec{u}^*)) = \vec{f}^n - \vec{\nabla}p^n, \tag{3}$$

$$\vec{\nabla}\cdot\vec{\nabla}\delta p^{n+1} = \frac{3}{2\delta t_n}\vec{\nabla}\cdot\vec{u}^*, \tag{4}$$

$$p^{n+1} = p^n + \delta p^{n+1}, \tag{5}$$

$$\vec{u}^{n+1} = \vec{u}^* - \frac{2\delta t_n}{3}\vec{\nabla}\delta p^{n+1} \tag{6}$$

where $n+1$ is the current time step, n and $n-1$ represent the previous and preprevious time step, respectively. $\vec{u}^*$ is an intermediate velocity which may not satisfy the continuity condition (2) and δt denotes the time step size.
Of special interest here is the wall treatment. In the code, the wall node is shifted to a wall distance $y(1) \equiv y_\delta$ being now the new first node above the wall. Denote $y(2)$, $y(3)$ the wall distance of the second and third off-wall node after shifting, and $V(1)$, $V(2)$, $V(3)$ the corresponding control volumes with faces at $y_{12} = (y(1)+y(2))/2$ and $y_{23} = (y(2)+y(3))/2$. We choose $y_\delta \equiv y(1) = 0.27y(2)$ as a compromise to balance the two requirements that $y(1)$, $y(2)$ should be close to the center of their respective control volumes $V(1)$, $V(2)$, see Figure 1 (right).
Denote Γ_w the wall and Γ_δ an artificial inner boundary containing the shifted nodes at wall distance y_δ. The use of Γ_δ in (8) will be motivated further in Subsection 2.3 below. Then, as a boundary condition on Γ_w, the wall-shear

stress τ_{w} is prescribed instead of no-slip:

$$\vec{u}\cdot\vec{n}=0,\quad (\mathbb{I}-\vec{n}\otimes\vec{n})2\nu\mathbb{S}(\vec{u})\vec{n}=-\tau_{\mathrm{w}}\vec{u}_{\mathrm{t},\delta}\quad \text{on}\quad \Gamma_{\mathrm{w}}\ . \tag{7}$$

with $\mathbb{I}-\vec{n}\otimes\vec{n}$ being the projection operator onto the tangential space of Γ_{w}, unit velocity vector in wall-parallel direction $\vec{u}_{\mathrm{t},\delta}=\vec{v}_{\mathrm{t},\delta}/|\vec{v}_{\mathrm{t},\delta}|$ and

$$\tau_{\mathrm{w}}=\nu\vec{\nabla}u_\delta\cdot\vec{n}\ ,\quad \text{where}\quad u_\delta\ =\ |\vec{v}_{\mathrm{t},\delta}|\ ,\quad \vec{v}_{\mathrm{t},\delta}=(\mathbb{I}-\vec{n}\otimes\vec{n})\,\vec{u}|_{\Gamma_\delta}\ . \tag{8}$$

For LES of turbulent flows, the basic Navier-Stokes model (1)-(2) has to be modified. In LES, a scale separation operator subdivides the scales into filtered scales and unresolved scales. Only the filtered scales are solved. In this work the effects of the unresolved scales are modeled by a sub-grid stress (SGS) term of so-called eddy-viscosity type.

2.1 Smagorinsky model

In this classical LES model, viscosity ν is replaced by $\nu+\nu_t$. The eddy-viscosity ν_t is given by

$$\nu_{\mathrm{t}}=(C_S\Delta)^2|\mathbb{S}|\ ,\qquad |\mathbb{S}|=(2\mathbb{S}:\mathbb{S})^{1/2} \tag{9}$$

with $\mathbb{A}:\mathbb{B}=\sum_{i,j=1}^{d}A_{ij}B_{ij}$. Therein the filter width Δ is given by $\Delta=nh_{\mathrm{c}}$, with $h_{\mathrm{c}}=\mathrm{Vol}_{\mathrm{c}}^{1/3}$, where $\mathrm{Vol}_{\mathrm{c}}$ is the volume of the control volume surrounding $\vec{x}$ and $n=1,2,\ldots$. The model constant to be calibrated is C_S.
Near solid walls, the turbulent viscosity ν_{t} is multiplied with the van Driest damping function $D(y^+)$. For $\vec{x}\in\Omega$, denote $\vec{x}_{\mathrm{w}}=\vec{x}_{\mathrm{w}}(\vec{x})\in\Gamma_{\mathrm{w}}$ the corresponding nearest wall point with distance d from $\vec{x}$. Then

$$D(y^+)=(1-\exp(-y^+/A^+))^2\ ,\quad y^+=yu_\tau/\nu\ ,\quad u_\tau=u_\tau|_{\vec{x}_w}=\sqrt{\tau_{\mathrm{w}}} \tag{10}$$

with friction velocity u_τ, $y=\mathrm{dist}(\vec{x},\vec{x}_w(\vec{x}))\equiv d$ and $A^+=26$. Due to its non-local character van Driest damping is not very suitable for unstructured methods or if parallelisation is used.

2.2 Detached-eddy simulation model

Detached-eddy simulation (DES) is a single non-zonal hybrid RANS-LES method [34]. The SA-DES is based on the one-equation RANS model by Spalart & Allmaras which computes the eddy viscosity $\nu_{\mathrm{t}}=f_{v1}\tilde{\nu}$ from the auxiliary viscosity $\tilde{\nu}$ using a near-wall damping function $f_{v1}=\chi^3/(\chi^3+c_{v1}^3)$ with $\chi=\tilde{\nu}/\nu$ which involves only local variables. Here $\tilde{\nu}$ solves the transport equation

$$\partial_t\tilde{\nu}+\vec{u}\cdot\vec{\nabla}\tilde{\nu}-\vec{\nabla}\cdot\left(\frac{\nu+\tilde{\nu}}{\sigma}\vec{\nabla}\tilde{\nu}\right)-\frac{c_{b2}}{\sigma}(\vec{\nabla}\tilde{\nu})^2\ =\ c_{b1}\tilde{S}\tilde{\nu}-c_{w1}f_w(\frac{\tilde{\nu}}{d})^2$$

with $\tilde{S}=|\Omega|+\tilde{\nu}/(\kappa^2d^2)f_{v2}$, $|\Omega|=(2\Omega(\vec{u}):\Omega(\vec{u}))^{1/2}$, and $\Omega(\vec{u})=(\vec{\nabla}\vec{u}-(\vec{\nabla}\vec{u})^T)/2$. The functions f_w, f_{v2} and the constants $\sigma, c_{b2}, c_{b1}, C_{w1}$ are given in

[34].
In the SA-DES model, the wall distance d is replaced by

$$\tilde{d} \;=\; \min(\, d \,,\; C_{DES}\Delta) \quad \text{with} \;\; \Delta = \max(\Delta x, \Delta y, \Delta z). \tag{11}$$

The model constant to be calibrated is C_{DES}.

2.3 Near-wall treatment for LES at high Reynolds numbers

Wall-functions are used to bridge the near-wall region at high Reynolds numbers. The wall shear stress τ_{w} can be computed from (8) only if $y_\delta^+ < 2$. For larger y_δ^+, $\tau_{\mathrm{w}} = u_\tau^2$ is computed from friction velocity u_τ: The universal velocity profile of RANS-type by Reichardt $F(y^+)$ is matched with the instantaneous LES solution u_δ at the shifted node y_δ

$$\frac{u_\delta}{u_\tau} = F\left(\frac{y_\delta u_\tau}{\nu}\right) \;, \quad F(y^+) \equiv \frac{\ln(1+0.4y^+)}{\kappa} + 7.8\Big(1 - e^{-\frac{y^+}{11.0}} - \frac{y^+}{11.0} e^{-\frac{y^+}{3.0}}\Big) \;. \tag{12}$$

Equation (12) is solved for u_τ using Newton's method. In the implementation a single formula for an auxiliary eddy viscosity ν_{rd} at the shifted node y_δ is used to compute τ_{w}

$$\tau_{\mathrm{w}} = \nu_{\mathrm{rd}} \frac{u_\delta}{y_\delta} \;, \quad \nu_{\mathrm{rd}} = \nu \max\left(1, \frac{y^+}{F(y^+)}\right) \tag{13}$$

For $y_\delta^+ < 2$, $\nu_{\mathrm{rd}} = \nu$ and (13) reduces to (8). In the general case, (13) can be rewritten as $\tau_{\mathrm{w}} = \nu(y_\delta^+/u_\delta^+)(u_\delta/y_\delta) = u_\tau^2$.
We remark that (12) is an approximative solution of the boundary layer equation for (magnitude of) wall-parallel velocity in wall-normal direction using the stress equilibrium assumption, i.e., neglecting convective and pressure gradient term. Then, for each $\vec{x}_{\mathrm{w}} \in \Gamma_{\mathrm{w}}$ and given u_δ seek the wall-parallel component of velocity $u^{\mathrm{RANS}}(y)$ such that

$$\frac{\mathrm{d}}{\mathrm{d}y}\Big((\nu + \nu_{\mathrm{t}}^{\mathrm{RANS}})\frac{\mathrm{d}}{\mathrm{d}y}u^{\mathrm{RANS}}\Big) = 0 \quad \text{in} \quad \{\, \vec{x}_{\mathrm{w}} - y\vec{n} \mid y \;\in\; (0, y_\delta)\} \tag{14}$$

$$u^{\mathrm{RANS}}(0) \;= 0 \;, \qquad u^{\mathrm{RANS}}(y_\delta) \;=\; u_\delta \;. \tag{15}$$

3 Evaluation tools for model calibration

It is desirable to treat the calibration problem of basic turbulence models within the framework of optimisation problems. Consider the abstract equation

$$A(q, u) = f \quad \text{in} \quad \Omega. \tag{16}$$

(here: quasi-stationary turbulent Navier-Stokes model) for the state variable u (here: velocity/pressure) in a Hilbert space V (here: $V \subseteq [H^1(\Omega)]^3 \times L^2(\Omega)$) with the parameter vector q (here: model and grid parameter) in the control space $Q := \mathbb{R}^{n_p}$. Let $C : V \to Z$ be a linear observation operator mapping u into the space of measurements $Z := \mathbb{R}^{n_m}$ with $n_m \geq n_p$. Then q is calculated from the constrained optimisation problem

$$\text{Minimize} \qquad J(q,u) := \frac{1}{2}\|C(u) - \hat{C}\|_Z^2 \tag{17}$$

with the cost functional $J : Q \times V \to \mathbb{R}$ under constraint (16) and using measurements $\hat{C} \in Z$. Assume the existence of a unique solution to (16)-(17) and of an open set $Q_0 \subset Q$ containing the optimal solution. Using the solution operator $S : Q_0 \to V$, one defines via $u = S(q)$ the reduced cost functional $j : Q_0 \to \mathbb{R}$ by $j(q) = J(q, S(q))$. The reduced observation operator $c(q) := C(S(q))$ leads to an unconstrained problem

$$\text{Minimize} \quad j(q) = \frac{1}{2}\|c(q) - \hat{C}\|_Z^2, \qquad q \in Q_0. \tag{18}$$

An efficient framework to the solution of the necessary optimality condition $j'(q) = 0$ of (18) provides the adjoint approach, see [16] for a review. The approach can be generalized to time-dependent problems. This makes the optimisation problem and solution techniques even much more expensive.
Techniques of (sub)optimal control have been applied to LES of turbulent channel flow in [35], see also the references given there. Different simplifications are made in order to reduce the computational costs of the adjoint approach. In particular, the turbulent viscosity ν_t is assumed to be solution–independent in the adjoint equation.
The simulation of turbulent flows with a statistically steady solution using a turbulence resolving model requires long time intervals. Although sophisticated tools such as a-posteriori based optimisation can reduce the costs, e.g. [6], recent optimisation tools for time-dependent problems are still extremely expensive regarding both CPU time and memory consumptions. Moreover, it is not yet clear how to treat the (nonlinear) turbulence model for the adjoint equation for time-dependent flows correctly.
As a conclusion of this discussion, a rather simple approach to the least-squares minimisation of the cost functional (18) is applied. As a basic step, a series of numerical simulations for a given flow problem will provide look-up tables for the cost functional depending on relevant model and grid parameters as a basis for further systematic considering. In some cases, a Newton type method is feasible to determine optimized parameters.

4 Calibration for decaying isotropic turbulence

The benchmark problem of decaying isotropic turbulence (DIT) mimics the experiment by [10] at a Taylor microscale Reynolds number $Re_\lambda \sim 150$. Here, it is used to select proper spatial discretisations of the convective term and to calibrate basic parameters of the LES and the SA-DES turbulence models.
For the DIT problem, we choose a cubic box domain $\Omega = (0, 2\pi)^3$ and an equidistant mesh with N^3 nodes. As initial condition, we use a divergence-free velocity field with energy spectrum $E(\kappa)|_{t=0}$ ($\kappa = |\vec{\kappa}|$, $1 \le \kappa \le M$, $M = N/2 - 1$) given by data in [10] which can be computed as

$$\vec{u}(\vec{x})|_{t=0} \;=\; \sum_{\substack{\kappa_1=0 \\ |\vec{\kappa}|\le\kappa_{\max}}}^{M} \sum_{\kappa_2,\kappa_3=-M}^{M} \Big(\frac{E(\kappa)|_{t=0}}{S_\kappa}\Big)^{1/2} 2\Big(\mathbb{I} - \frac{\vec{\kappa}\otimes\vec{\kappa}}{|\vec{\kappa}|^2}\Big)\vec{\gamma}(\vec{\kappa})\cos(\vec{\kappa}\cdot\vec{x} + \Theta(\vec{\kappa})).$$

The components of $\vec{\gamma}(\vec{\kappa})$ are real random numbers with Gaussian distribution in $[0, 1]$, S_κ is the number of wave-vectors $\vec{\kappa}$ with $\kappa - 1/2 \le |\vec{\kappa}| \le \kappa + 1/2$ and $\Theta(\vec{\kappa})$ is a random phase with uniform distribution in $0 \le \Theta \le 2\pi$.
Denote $\langle\cdot\rangle$ the averaging operator over the three homogeneous directions. The expectation values of the velocity $\vec{U} = \langle\vec{u}\rangle$ (mean velocity) as relevant first order flow statistics are constant for fixed time and therefore not of interest. The turbulent kinetic energy $k = \frac{1}{2}\langle(\vec{u} - \langle\vec{u}\rangle)^2\rangle$ represents second order statistics. It can be characterized in Fourier space via the energy spectral density

$$k(t) = \sum_{\kappa=0}^{M} E(\kappa, t)\ , \quad E(\kappa, t) = \sum_{\kappa-\frac{1}{2}<|\vec{q}|\le\kappa+\frac{1}{2}} \frac{1}{2}\hat{\vec{u}}(\vec{q}, t)\cdot\hat{\vec{u}}^*(\vec{q}, t)\ , \qquad (19)$$

with $\kappa = 1, 2, \ldots, M$, where $\hat{\vec{u}}^*$ denotes the complex conjugate of $\hat{\vec{u}}$

$$\hat{\vec{u}}(\vec{\kappa}, t) \;=\; \frac{1}{N^3}\Big(\sum_{x_1,x_2,x_3=0}^{N-1} \vec{u}(\vec{x}, t)\cos(-\vec{\kappa}\cdot\vec{x}) + i\sum_{x_1,x_2,x_3=0}^{N-1} \vec{u}(\vec{x}, t)\sin(-\vec{\kappa}\cdot\vec{x})\Big). \qquad (20)$$

We consider experimental data for $t = 0.87$[s] and $t = 2.0$[s] by [10]. Therefore, the cost functional (depending on some parameter C) is based on a discrete least-squares functional for the energy spectral density:

$$J(C) \;=\; \Big(\sum_{i=1}^{M}\Big[(E(\kappa_i, C) - E_{\exp}(\kappa_i))^2_{t=0.87[\mathrm{s}]} \;+\; (E(\kappa_i, C) - E_{\exp}(\kappa_i))^2_{t=2.0[\mathrm{s}]}\Big]\Big)^{1/2}.$$

The model parameter C_S resp. C_{DES} and the filter width Δ (more precisely, the ratio Δ/h with mesh size h) play an important role in the modelling. In a preliminary study (with $N \le 64$) not given here, best results were obtained for$\Delta/h = 2$.
The time step size used was $\delta t = 0.0087[s]$. Additional simulations with a time step size which was 5 times and 10 times smaller showed that temporal

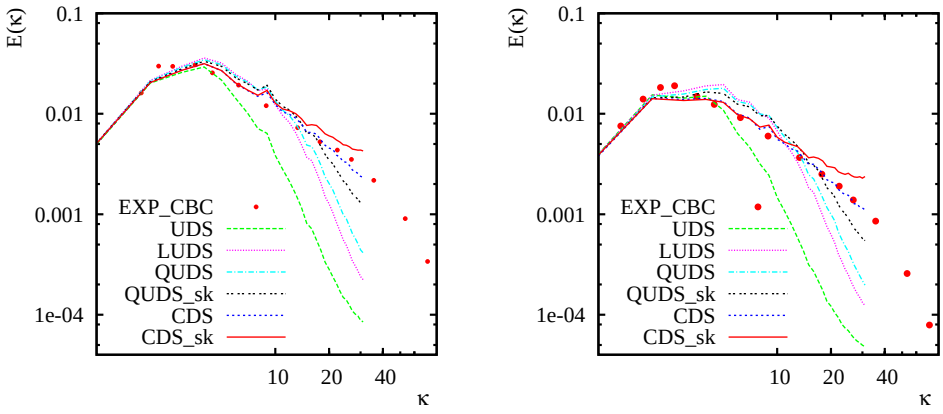

Fig. 2. Testcase DIT on 64^3 mesh. Energy spectrum at $t = 0.87$[s] (left) and $t = 2.0$[s] (right) for $C_S = 0.1$.

discretization errors are insignificant. Then different discretisations and formulations of the convective term are studied. We consider the divergence form $\vec{\nabla} \cdot (\vec{u} \otimes \vec{u})$ and the skew-symmetric form $\frac{1}{2}\vec{\nabla} \cdot (\vec{u} \otimes \vec{u}) + \frac{1}{2}[(\vec{u} \cdot \vec{\nabla})\vec{u} + (\vec{\nabla} \cdot \vec{u})\vec{u}]$, which are analytically but not computationally equivalent, see e.g. [20]. Figure 2 shows the computed energy spectra at $t = 0.87$[s] (left) and $t = 2.0$[s] (right) for $C_S = 0.1$ and $N = 64$. Only the central discretisation (CDS) with divergence form is suitable to resolve the large wave-number part of the spectrum appropriately, whereas the upwind schemes LUDS and also the higher order QUDS produce excessive damping at high wave-numbers. Combining QUDS with a skew-symmetric formulation (QUDS_sk) for the convective fluxes gives some improvement for the DIT test case, but poor results for the turbulent channel flow at $Re_\tau = 395$, see next section. For CDS with skew-symmetric form, too much energy is contained in the high wave numbers. For more details we refer to [38].

Figure 3 (left) shows the dependence of the cost functional on the Smagorinsky constant $C = C_S$ for $N = 64$. A Newton-type method (based on numerical differentiation) delivers a global minimum with $C_S = 0.094$ for CDS and $C_S = 0.123$ for QUDS_sk. The value for CDS is in close agreement with $C_S = 0.085$ from literature (using $\Delta/h = 2$), see [28]. For the SA-DES model a similar Newton-type approach yields a global minimum of the functional for $C = C_{DES} = 0.67$. This result might seem to be just confirmatory. But it is important to note that low-order methods typically used by industry can suffer from too large numerical dissipation at the large wave numbers if the underlying numerical methods are not appropriate. Then altered, i.e. lower, values for the above model constants are used in order to obtain a better agreement with the energy spectra, see e.g. [15]. Therefore the fact that the standard values are obtained confirms that the underlying numerical method is appropriate. In Figure 3 (right), the energy spectrum for Smagorinsky model and SA-DES model using CDS with optimized values for C_S and C_{DES} respectively are shown for $N = 64$ and the agreement with the experimental

data is very satisfying.

Results on a 128^3 mesh are shown in Figure 4. Simulations on the fine

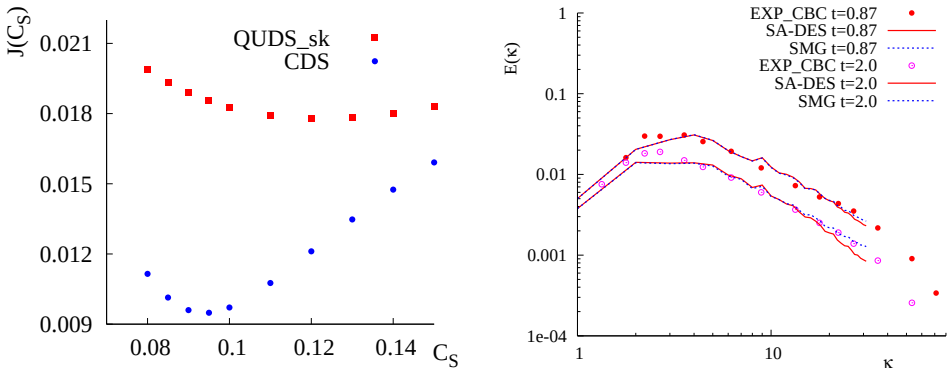

Fig. 3. Testcase DIT on 64^3 mesh. Left: Calibration of Smagorinsky constant C_S. Right: Energy spectrum for optimized C_S resp. C_{DES} for CDS scheme.

mesh give a minimum for J at $C_S = 0.09$, but values for J in the range $C_S \in \{0.08, 0.1\}$ are close. Spectra for $C_S = 0.094$ for $N = 64$ and $C_S = 0.1$ for $N = 128$ (see Figure 4 (right)) show that the $k^{-5/3}$ range is relatively small for the present low Reynolds number. As a consequence of these results,

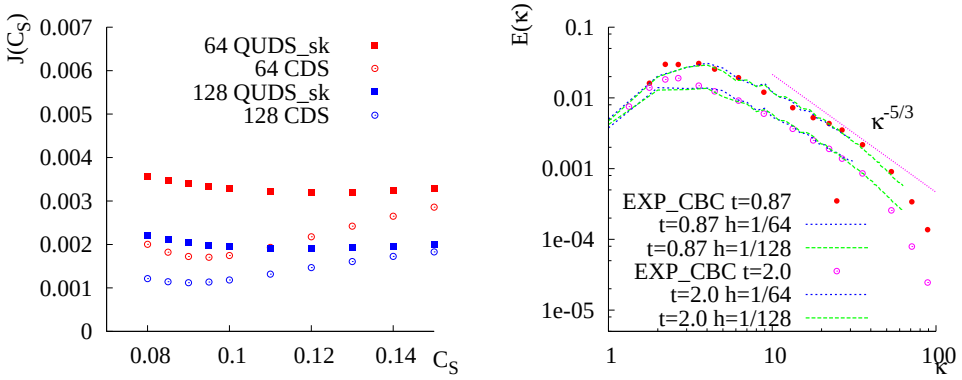

Fig. 4. Testcase DIT on 128^3 mesh. Left: Calibration of Smagorinsky constant C_S. Right: Energy spectrum using $C_S = 0.094$ for $N = 64$ and $C_S = 0.1$ for $N = 128$.

only the CDS scheme for the convective term in divergence form and the ratio $\Delta/h = 2$ are considered in further simulations.

Finally, the mesh convergence of the results is addressed. For this purpose, we consider $\epsilon_{(0,\kappa)}$ which describes the dissipation in wavenumbers less than κ, see [28] p.189. From this quantity, the corresponding Kolmogorov scale $\eta = \eta_{(0,\kappa)}$ is computed, see [28] p.128, which is given by

$$\eta_{(0,\kappa)} = \left(\nu^3/\epsilon_{(0,\kappa)}\right)^{1/4} , \quad \epsilon_{(0,\kappa)} = \int_0^\kappa 2\nu\kappa'^2 E(\kappa')\mathrm{d}\kappa' .$$

This allows to assess convergence of the results in a spectral sense, see Figure 5. For each $\kappa = 15, 31, 63$, it can be seen that the numerical value of $\eta_{(0,\kappa)}$ comes closer to the experimental value if N is increased. This indicates convergence

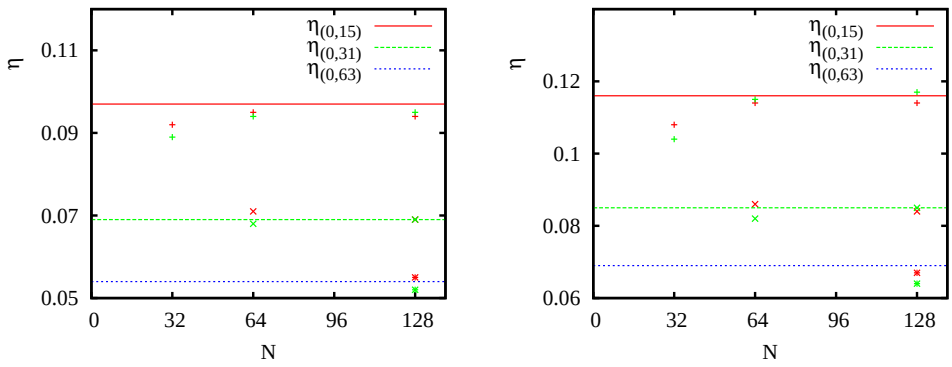

Fig. 5. DIT: Mesh convergence of Kolmogorov scale $\eta = \eta_{(0,\kappa)} = (\nu^3/\epsilon_{(0,\kappa)})^{1/4}$ derived from $\epsilon_{(0,\kappa)}$ for $t = 0.87[s]$ (left) and $t = 2.0[s]$ (right). Symbols denote $+$: $\eta_{(0,15)}$, $\times$: $\eta_{(0,31)}$, $*$: $\eta_{(0,63)}$. For each pair $(N, \eta_{(0,\kappa)})$ two values are shown, viz., for $C_S = 0.09$ and $C_S = 0.10$. Horizontal lines are the experimental value.

in a spectral sense. Moreover, for larger N the sensitivity (i.e., the spreading) of the predicted value of $\eta_{(0,\kappa)}$ with respect to different values for the model parameter C_S (here: $C_S = 0.09$ and $C_S = 0.1$) becomes smaller. Finally, it can be clearly seen that the results for $\eta_{(0,15)}$ and $\eta_{(0,31)}$ on the 64^3-mesh are already very close to the results for the 128^3-mesh. This supports to perform the parameter calibration study on the 64^3-mesh.

5 Calibration for channel flow

In this section, we consider LES and DNS for the benchmark problem of fully developed turbulent channel flow in the domain $\Omega = (0, 2\pi) \times (0, 2) \times (0, \pi)$. Periodic boundary conditions in streamwise x-direction, a no-slip condition for the walls in y-direction and symmetry planes in the spanwise z-direction are imposed.

5.1 Channel flow at $Re_\tau = 395$

First, we consider a moderate Reynolds number $Re_\tau = u_\tau H/\nu = 395$ with channel half width $H = 1$, for which DNS data are available [25]. In order to achieve a constant mass flux, the streamwise forcing term is adjusted dynamically by taking into account the time step size δt_n and the bulk velocity from the DNS data and the actual bulk velocity at the present time t_n

$$\vec{f} \;=\; \tau_{\mathrm{w}}\vec{e}_x \;+\; \frac{1}{\delta t_n}(U_{\mathrm{bulk,DNS}} - U_{\mathrm{bulk}}(t)) \;, \quad U_{\mathrm{bulk}} = \frac{1}{H}\int_0^H u(y)\mathrm{d}y \qquad (21)$$

where $\vec{e}_x$ denotes the unit-vector in x-direction. As initial condition we use a randomly perturbed approximative RANS solution $\vec{u}|_{t=0} = u_\tau F(du_\tau/\nu)\vec{e}_x + 0.1U_{\mathrm{bulk}}\vec{\psi}$ where d is the wall distance, F is given by (12) and each component of $\vec{\psi}$ is a random number in $(-1, 1)$. The Smagorinsky constant C_S as model

parameter and $y^+(1)$ as grid parameter are the quantities that we want to identify via sampling of the cost functionals.
The spatial discretisation uses $N_x \times N_y \times N_z = N^3$ nodes with $N = 24, 32, 48, 64, 96$. For $N = 64$, the equidistant spacing in x- and z-direction corresponds to $\Delta x^+ = \Delta x u_\tau/\nu = 38.8$ and $\Delta z^+ = \Delta z u_\tau/\nu = 19.4$ respectively. The grid in wall-normal direction is stretched using a hyperbolic tangent function

$$\frac{y(j)}{H} \;=\; \frac{\tanh[\gamma(2j/N_y - 1)]}{\tanh(\gamma)} \;+\; 1.0\;, \quad j = 0, 1, \ldots, N_y \tag{22}$$

where $y(j)$ is the coordinate of the jth grid point in y-direction providing thus an anisotropic, layer-adapted mesh, see [24]. The stretching parameter γ is taken to be $\gamma \in \{1.2, 1.5, 1.72, 2.2\}$ which corresponds to $y^+(1) \in \{0.39, 0.79, 1.06, 1.45\}$ for the shifted wall node (for $N = 64$). The computational time step is chosen as $\delta t^+ \equiv \delta t u_\tau^2/\nu = 0.4$. After reaching a statistically steady solution, first-order and second-order statistics are computed. Denote $\langle\cdot\rangle$ the averaging operator over the two homogeneous directions and in time. 8000 time steps are performed to let the flow develop and reach the statistically steady state, statistics are collected over another 6000 steps. The quantities of interest are the mean velocity in streamwise direction $U = \langle\vec{u}\rangle \cdot \vec{e}_x$, the turbulent kinetic energy $k = \frac{1}{2}\langle(\vec{u} - \langle\vec{u}\rangle)^2\rangle$ and their normalized variants $U^+ = \frac{U}{u_\tau}$ and $k^+ = \frac{k}{u_\tau^2}$.
In a preliminary study not given here, it was observed that the results with QUDS resp. QUDS_sk and also the results with first-order accurate time discretisation scheme with CDS are not satisfying. However the statement regarding the skew-symmetric form may also depend on the treatment of pressure [20].
As a first step the role of the spatial and temporal discretisation error was studied. Turbulence statistics from simulations with $\delta t^+ = 0.4$ are sufficiently close to those from computations with $\delta t^+ = 0.2$, see Figure 6, confirming results by [8].

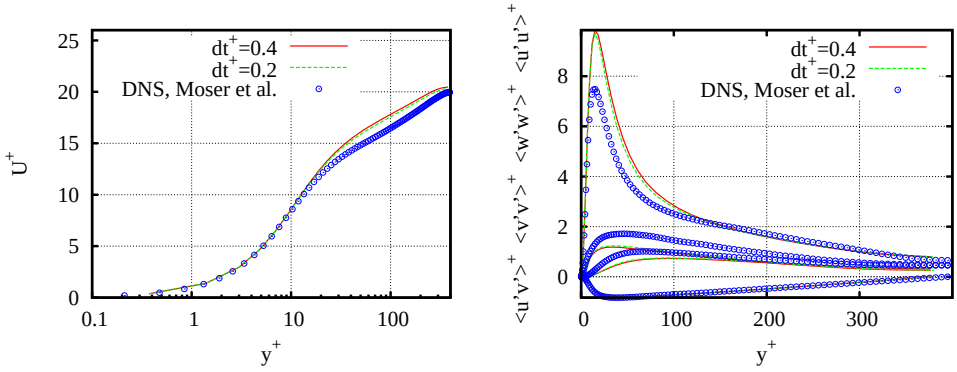

Fig. 6. Influence of time step size on mean velocity (left) and fluctuations (right) for channel flow at $Re_\tau = 395$ using SMG model on 64^3-mesh with $y^+(1) = 0.39$.

In order to assess grid convergence, simulations on meshes with N^3 nodes

with $N = 24, 32, 48, 64, 96$ for the Smagorinsky model with standard value for channel flow $C_S = 0.05$ are considered. Figure 7 shows that on the finest mesh $N = 96$ results are much closer to the DNS data than for $N = 64$, in agreement with the notion in [24].

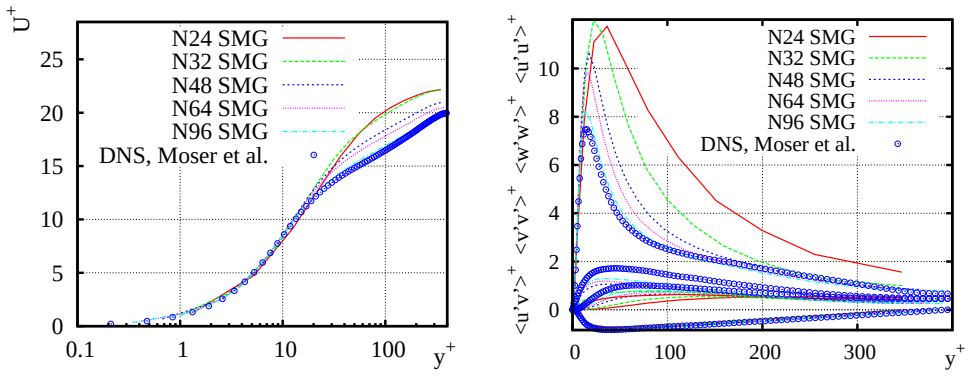

Fig. 7. Convergence study for channel flow at $Re_\tau = 395$ using SMG model on $N \times N \times N$-meshes with $N = 24, 32, 48, 64, 96$ and $y^+(1) = 0.39$. Left: Mean velocity. Right: Fluctuations.

For the parameter optimization the l^2-error functional of the LES results compared to the DNS data for U and k are defined by

$$J_u(y^+(1), C) = \left(\sum_{j=0}^{N} (U_j(y^+(1), C) - U_{j,\mathrm{DNS}})^2 \Delta y_j \right)^{1/2} \tag{23}$$

$$J_k(y^+(1), C) = \left(\sum_{j=0}^{N} (k_j(y^+(1), C) - k_{j,\mathrm{DNS}})^2 \Delta y_j \right)^{1/2} \tag{24}$$

with $\phi_j = \phi(y(j))$ and spacing Δy_j in y-direction of cell j. The parameter space $\{C_S, y^+(1)\}$ is now two-dimensional and too large to compute the entire look-up table on the 96^3 meshes. Therefore the following two-step optimization strategy is used. First we perform a (precursor) optimization using the relatively coarse 64^3 mesh. This first step is to reduce the parameter range. J_u and J_k are almost constant for $C_S \in [0, 0.10]$ and $y^+(1) \in [0.5, 1.5]$ and become smallest for $C_S \in [0, 0.06]$, see Figure 8. In the second step we perform fine grid LES on the 96^3 mesh in order to find the optimal parameter C_S not effected significantly by the numerical error. Here we only investigate the reduced parameter range $\{C_S, y^+(1)\}$ with $C_S \in [0, 0.10]$ and fixed $y^+(1) = 0.39$. For the cost functionals, no distinct minimum can be concluded, but there is a plateau of minimum values for J_u in the range $0 \leq C_S \leq 0.06$. This is supported by the observation that the profiles for mean flow and statistics almost coincide for $C_S \in \{0.01, 0.03, 0.05\}$, and also the relative error in u_τ w.r.t. the imposed value is also almost constant.

It is well known that the standard optimal value for the Smagorinsky model $C_S = 0.05$ for $\Delta/h = 2$ differs from the optimal value for DIT, see [28]. The present results do not disagree with this standard choice, although J_u and J_k

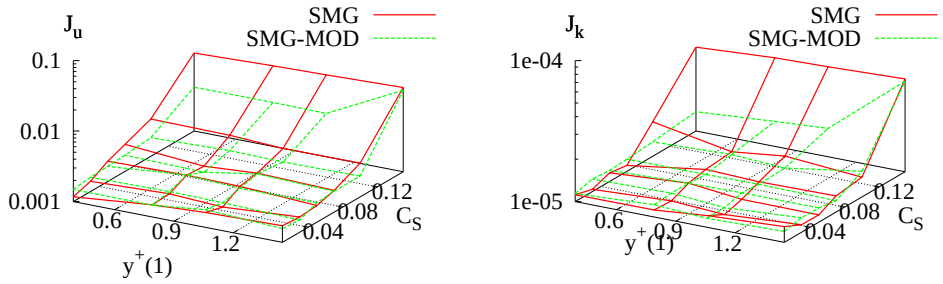

Fig. 8. Cost functionals for channel flow $Re_\tau = 395$ on 64^3-mesh, Left: mean velocity. Right: kinetic energy.

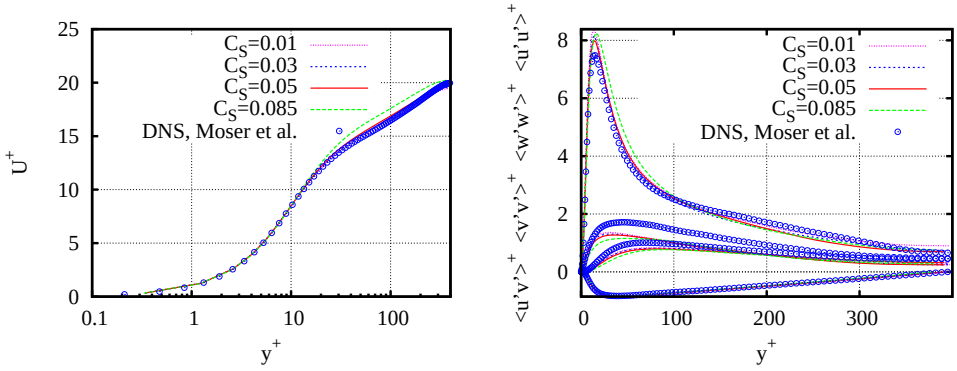

Fig. 9. Variation of C_S for channel flow at $Re_\tau = 395$ using SMG model on 96^3-mesh. Left: Mean velocity. Right: Fluctuations.

do not show a distinct minimum for $C_S = 0.05$.

5.2 Application to channel flow at higher Re_τ

Now, the goal is to simulate turbulent channel flow at $Re_\tau = 4800$ using the calibrated model parameters. Numerical results are compared also with experimental data by Comte-Bellot from [2], but these should be seen with caution, since for the three cases considered ($Re_\tau = 2340$, 4800, 8160) the values obtained for slope $1/\kappa$ and constant C of the log law $u^+ = \log(y^+)/\kappa + C$ show a relatively large spreading and also differ from the standard values. As a wall-resolved LES (as for $Re_\tau = 395$) is very expensive due to the much finer mesh not only in wall-normal direction, but also in streamwise and spanwise direction in conjunction with a much smaller time step, wall functions (see Subsec. 2.3) are used together with the Smagorinsky model (WSMAG).
First the role of the time discretisation error is studied on a mesh with $96 \times 24 \times 96$ nodes and $y_\delta^+ = 50$ for the (shifted) first node above the wall, see Figure 10. For $Re_\tau = 4800$, $\Delta t = 0.02$, 0.01, 0.005, 0.0025 correspond to $\delta t^+ = 7.0$, 3.5, 1.75, 0.875. The statistics are sampled over 10,000 time steps after 10,000 steps flow developing (for $\delta t^+ = 7$). Recall that $\delta t^+ = 0.4$ was

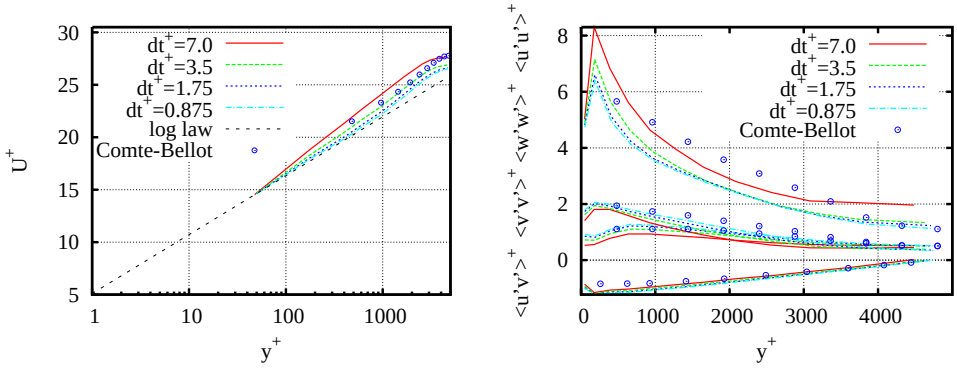

Fig. 10. Time-discretisation error for Smagorinsky model with near-wall modelling (WSMG) for channel flow at $Re_\tau = 4800$, Left: Mean velocity. Right: Fluctuations.

required for sufficiently small time discretisation error for wall-resolved LES at $Re_\tau = 395$. For $Re_\tau = 4800$ using wall-functions, $\delta t^+ = 1.75$ is required to ensure that time discretisation error is sufficiently small. This is only a factor of four larger compared to wall resolved LES. The second observation is that the log-layer mismatch is most pronounced for the too large δt and can be reduced largely by decreasing δt.
Secondly the role of the spatial discretisation error is studied, see Figure 11. Three meshes are considered with $N_x \times N_y \times N_z$ nodes where $N_x = N_z \in$

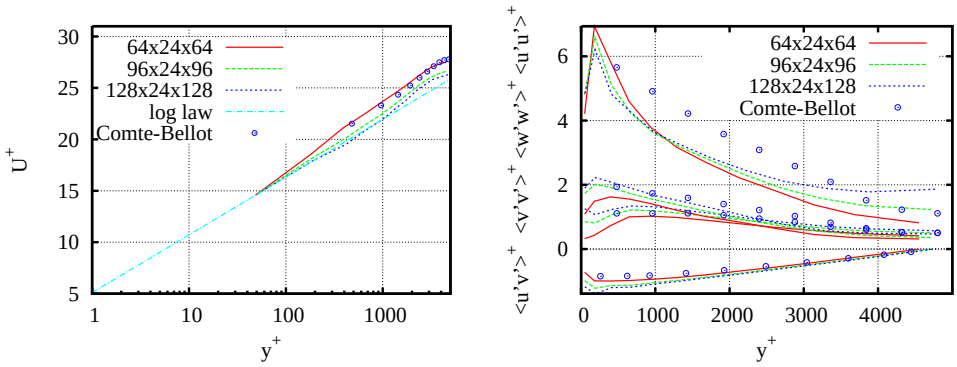

Fig. 11. Study of spatial discretisation error for Smagorinsky model with near-wall modelling (WSMG) for channel flow at $Re_\tau = 4800$ using $\delta t^+ = 1.75$, Left: Mean velocity. Right: Fluctuations.

$\{64, 96, 128\}$ corresponding to $\Delta x^+ = 2\Delta z^+ = 470, 317, 235$. For $N_x = 64$ streamwise fluctuations are largely overpredicted showing an underresolved LES, see [18]. Results on the two meshes $N_x = 96$ and $N_x = 128$ are close. However, they differ in the channel center, since spacing in the channel center is relatively coarse. The spacing in x- and z-direction is relatively coarse even for $N_x = 128$, cf. [31], but mesh convergence of the results is judged to be already satisfactory.

6 Flow over backward facing step at $Re_h = 37500$

In this section we consider the turbulent flow over a backward-facing step at a higher Reynolds number $Re_h = U_0 h/\nu = 37500$ using wall functions. Experimental data by Driver and Seegmiller [11] are available. The length of the inflow part is $4h$, the channel height upstream is $8h$, where $h = 0.0127$[m] is the step height and the channel length after the step is 25h. The inflow centerline velocity is $U_0 = 44.2$[m/s].
Wall-functions are used at the upper and bottom walls and periodic boundary conditions in spanwise direction. The wall opposite the step was parallel to the wall in the experiment considered here. If we remove the upper half of the channel and treat the centerline as a symmetry plane, a RANS calculation using the Spalart-Allmaras model showed that the velocity at the outlet will slow down around 12% compared with the case using the full geometry. Therefore the full configuration has to be considered. A blending of DNS data [32] in the near-wall region and experimental data [11] otherwise is used for the mean velocity profile at the inflow boundary. The method by [19] is applied to generate turbulence structures at the inflow boundary.
Since wall functions are used, relatively coarse grids in the near-wall region can be used. A hyperbolic tangent function is adopted to generate anisotropic grid spacing in wall normal $y-$direction. The mesh is equidistant in $x-$ and $z-$direction and only a small stretching is applied in $x-$direction near the outlet.
First the role of the time step size is studied on a grid consisting of $169\times N_y\times 32$ nodes, where in wall-normal direction $N_y = 54$ for $x \leq 0$ and $N_y = 71$ for $x > 0$ (Δx^+, Δz^+ are given in Table 1). For the time step size we use $\delta t = 5\times 10^{-5}[s], 2\times 10^{-5}[s], 1\times 10^{-5}[s], 5\times 10^{-6}[s]$ corresponding to a factor of 100, 40, 20 and 10 compared to the DNS at $Re_h = 5100$ by [21] and we note that $\delta t = 1\times 10^{-5}[s] \simeq 0.035 h/U_0$. In Figures 12-14 the profiles of mean velocity and fluctuations for different time step sizes are shown at 8 cross sections where experimental data are available. The average is performed over a simulation time $348h/U_0$ and spanwise direction after a flow developing time $348h/U_0$, which is around 12 "flow through" times. The results for mean flow and statistics from simulations with $\delta t = 1\times 10^{-5}[s]$ and $\delta t = 5\times 10^{-6}[s]$ are very close, which can be seen also from C_f in Figure 15. The time discretisation error is therefore judged to be sufficiently small. Agreement with the experimental data is also satisfying.
Since wall functions are used, skin friction coefficient C_f is computed using (12). Figure 15 presents C_f in comparison with the experimental data. The uncertainties in C_f were assessed by [11] to be $\pm 8\%$ for a 95% confidence level (with an uncertainty of $\pm 15\%$ in the region of separated flow).
In order to study grid convergence, four meshes are considered, see Table 1. Mesh spacing in plus units at $x/h = -0.5$ and $x/h = 10$ is also given. We used $\delta t = 2\times 10^{-5}[s]$. Results in Figures 16-18 show that the solutions on

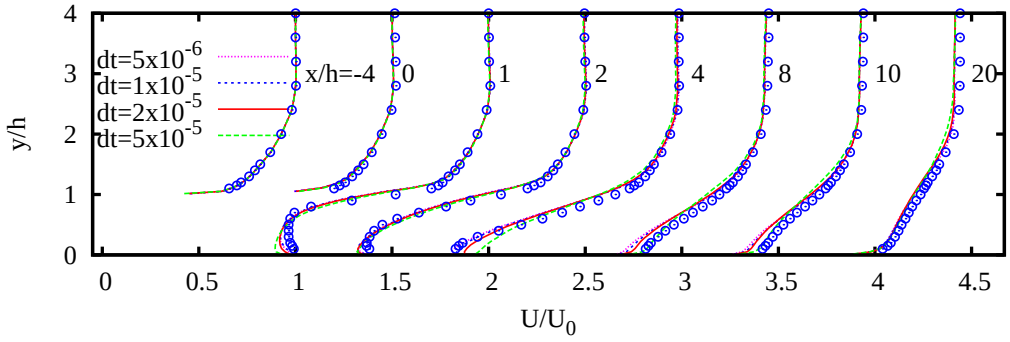

Fig. 12. Backward facing step at $Re_h = 37500$: Mean streamwise velocity for different time step sizes: ∘, exp. data of [11].

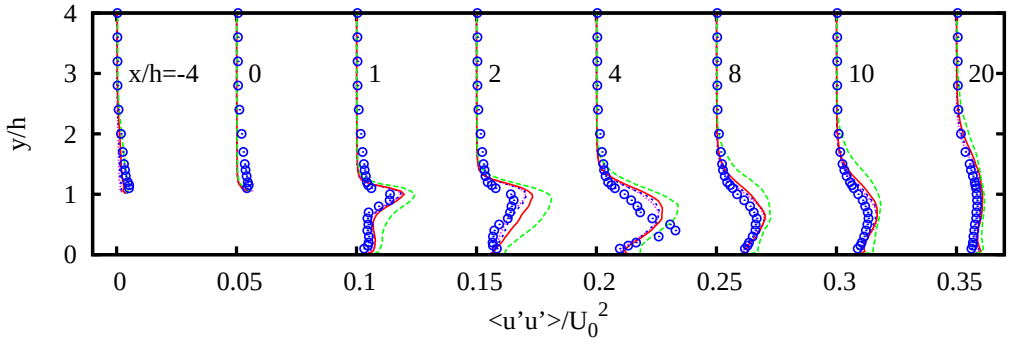

Fig. 13. Backward facing step at $Re_h = 37500$: Fluctuations $< u'u' >$ for different time step sizes: ∘, exp. data of [11]. Same line legend as in Figure 12.

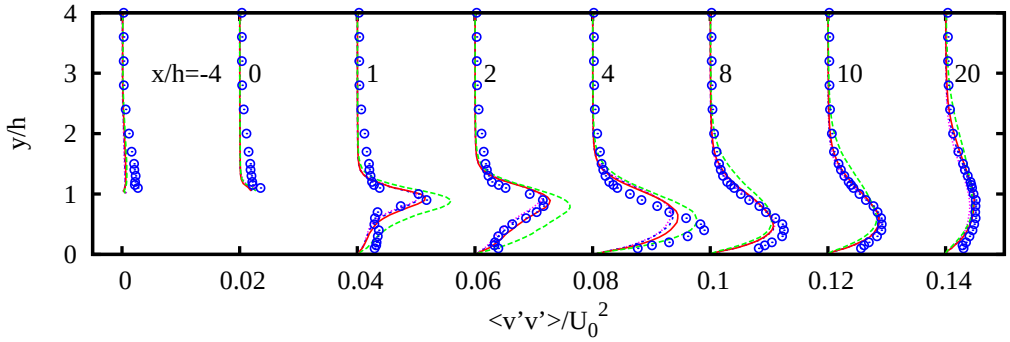

Fig. 14. Backward facing step at $Re_h = 37500$: Fluctuations $< v'v' >$ for different time step sizes: ∘, exp. data of [11]. Same line legend as in Figure 12.

the two coarser meshes deviate discernibly from the solution on the two fine meshes. This is at least in part due to the underresolved LES before the step which cannot maintain the turbulent structures in the boundary layer, which trigger the destabilisation of the shear layer downstream of the step and play an important role for the recirculation length, see e.g. [3,7]. On the positive

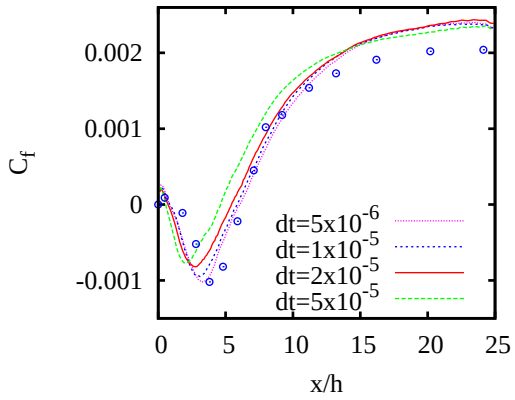

Fig. 15. Backward facing step at $Re_h = 37500$: Skin friction coefficient C_f for different time step sizes: ∘, exp. data of [11].

Table 1
Mesh spacing in plus unit for backward facing step at $Re_h = 37500$.

Mesh	78x31x16		110x47x32		169x71x32		219x89x32	
x/h	-0.5	10	-0.5	10	-0.5	10	-0.5	10
Δx^+	660	420	300	220	180	180	110	160
Δz^+	300	260	150	130	150	130	150	130

side, for the two fine meshes, the agreement with the experimental data is already satisfactory. It is worthwhile highlighting that the total simulation time is about 6 days on a single processor machine for the 169x71x32 mesh using $\delta t = 1 \times 10^{-5}[s]$.

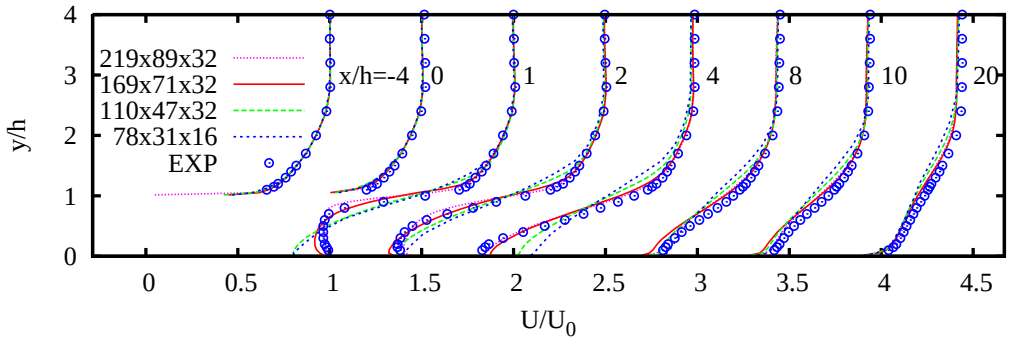

Fig. 16. Backward facing step at $Re_h = 37500$: Mean streamwise velocity on different meshes: ∘, exp. data of [11].

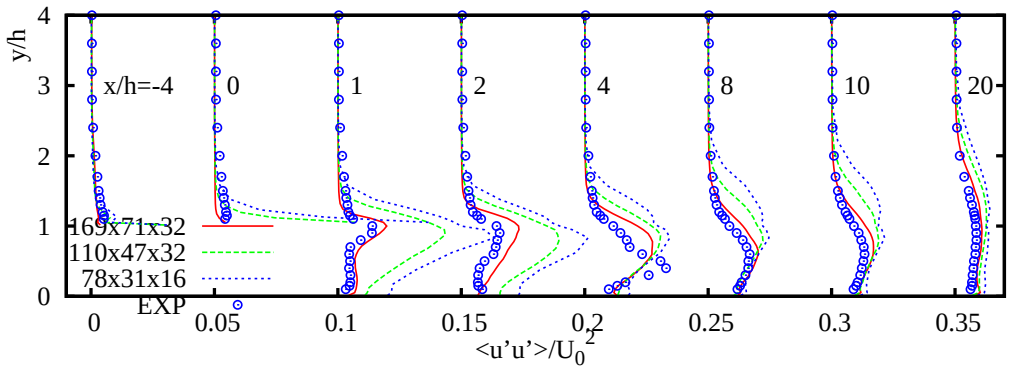

Fig. 17. Backward facing step at $Re_h = 37500$: Fluctuations $< u'u' >$ on different meshes: ∘, exp. data of [11].

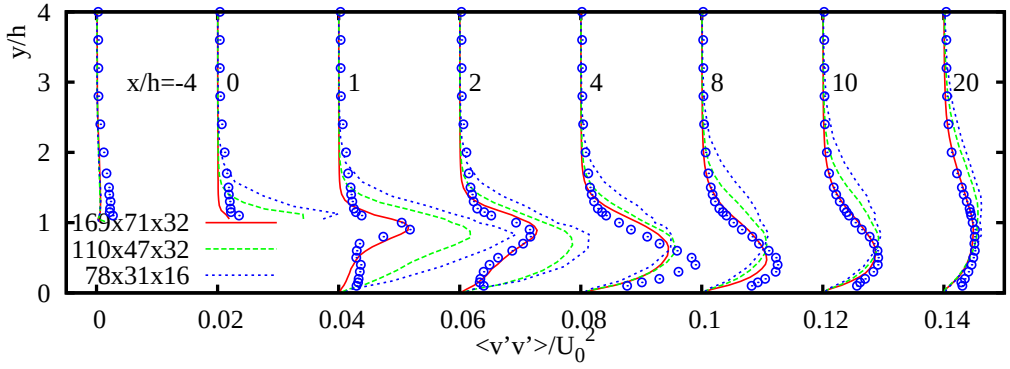

Fig. 18. Backward facing step at $Re_h = 37500$: Fluctuations $< v'v' >$ on different meshes: ∘, exp. data of [11].

7 Indicator for assessing the resolution quality of LES for free shear layers

The large influence of the spatial discretisation error on the quality of the LES results became obvious in the previous sections. This demands best practice guidelines for mesh design. Present results for LES with near-wall resolution (see Section 5.1) and wall-modelling using wall functions (see Sections 5.2, 6) confirm mesh requirements for attached boundary layer flow in streamwise, spanwise and wall-normal direction found in earlier studies, see [31] and references therein.

For free-shear layers and regions of separated flow, these guidelines cannot be applied. As a remedy, we now present a sensor S based on the resolved turbulent kinetic energy which measures the resolution quality of the LES in such flow regions. Based on the sensor value, the mesh can then be refined locally. The sensor S is designed such that it takes values in $[0, 1]$. $S > s_1$ indicates that mesh resolution is sufficiently fine and $S < s_0$ if the mesh is too coarse. The threshold values s_0, s_1 will be determined empirically below.

The concept of such a sensor was proposed by [29] with view on an *adaptive*

LES, where $\Delta = \Delta(x)$ is interpreted as a model parameter, and, if the ratio h/Δ is fixed, Δ is adapted by varying the mesh spacing until a desired turbulence resolution is obtained. As an abstract measure of turbulence resolution the fraction of the resolved to total turbulent kinetic energy is proposed. However, the turbulent kinetic energy in the residual or subgrid scale motion cannot be computed from resolved quantities and hence requires modelling, but no operational definition is given in [29]. For statistically steady flow, we propose

$$S(\vec{x}) \;=\; \frac{k}{k+k_{\rm sgs}}\;, \quad k=\frac{1}{2}\langle(\vec{u}-\langle\vec{u}\rangle)^2\rangle\;, \quad k_{\rm sgs}=\frac{1}{2}\langle(\vec{u}-\overline{\vec{u}})^2\rangle \tag{25}$$

where $\langle\cdot\rangle$ denotes the filtering operator in homogeneous directions and in time and $\overline{\vec{u}}$ is defined by the convolution integral

$$\overline{\vec{u}}(x,t) \;=\; \int_{\mathbb{R}^d} g_\Delta(\vec{x}-\vec{y})\vec{u}(\vec{y},t)\mathrm{d}\vec{y} \tag{26}$$

with g_Δ being the top hat filter function. The underlying idea is to use a scale similarity assumption for the subgrid scale velocity $\vec{u}_{\rm sgs}(\vec{x},t) \approx \vec{u}(\vec{x},t) - \overline{\vec{u}}(\vec{x},t)$. Since we are interested in S only remote from walls, there is no special adjustment of the filter definition for near-wall cells. The question whether an adaption of the filter definition at inflow and outflow boundaries is needed, requires additional investigation, but this is only fine tuning of the method.
Figures 19(a)-19(d) show sensor S for the turbulent flow over a backward facing step at $Re_h = 37500$ on the four meshes in Table 1. From Figures 16-18 we concluded that grid convergence on the two fine meshes is satisfactory but that the solution on the coarse mesh suffers from large error. For the coarse mesh $S < 0.8$ in large part of the free-shear layer and the recirculation region (see Figure 19(a)), but for the finest mesh $S > 0.85$ in the recirculation region and S around 0.9 in the free-shear layer (see Figure 19(d)). From this we suggest the threshold values $s_0 = 0.8$ and $s_1 = 0.9$. The separation between s_0 and s_1 should be large enough to make an automatic grid refinement method successful. Otherwise an additional scaling of the indicator could be used to make this distance larger.
Small sensor values in the channel center demonstrate that the sensor needs improvement for practical applications. In the channel center, k is small due to small turbulence production, since velocity gradients are small. As a remedy, an additional sensor hased on the mean flow (averaged over homogeneous directions and in time) is needed. The present mean flow is almost irrotational in the channel center, and the sensor (25)-(26) should be deactivated there.

8 Summary. Conclusions

In this paper we showed a validation strategy for enhancement of an unstructured industrial finite-volume solver designed for steady RANS problems for

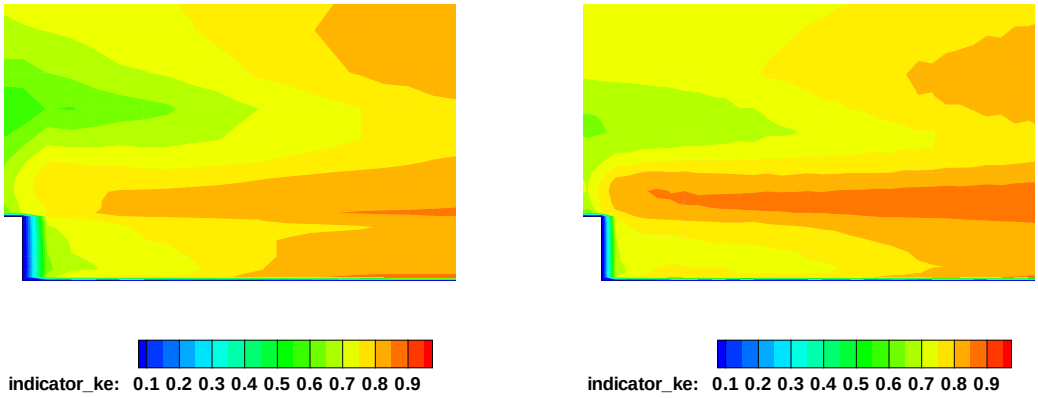

(a) WSMAG on $78 \times 31 \times 16$-mesh

(b) WSMAG on $110 \times 47 \times 32$-mesh

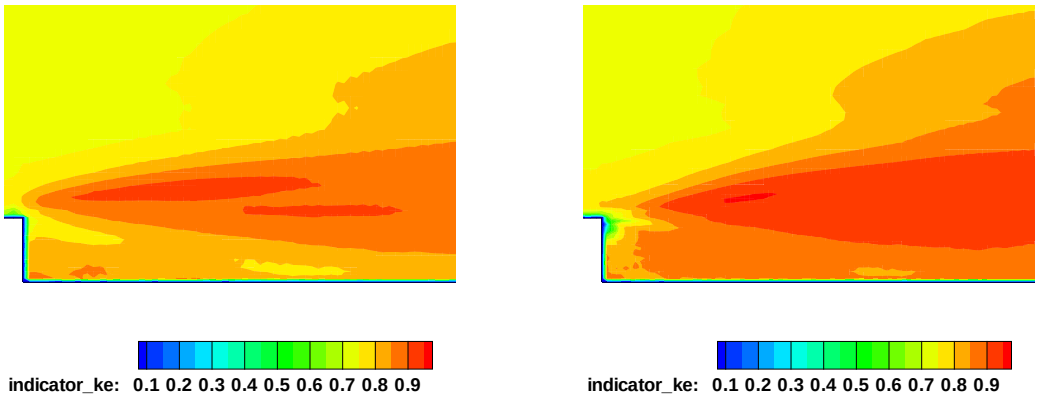

(c) WSMAG on $169 \times 71 \times 32$-mesh

(d) WSMAG on $219 \times 89 \times 32$-mesh

Fig. 19. Measure of turbulence resolution using sensor (25)-(26) for four different meshes for turbulent flow over a backward facing step at $Re_h = 37500$ using Smagorinsky model with wall-functions.

large eddy-type simulation with near-wall modelling of incompressible high-Reynolds number flow. Summary of the results and conclusions will be given by referring to the four questions raised in the introduction. Regarding the *first question* posed in the introduction we showed that it is possible to adopt second-order schemes to achieve LES capability. Key elements are using central difference scheme (CDS) for the convective term in divergence form and a second order accurate time discretisation using the BDF(2) scheme. For the benchmark cases of DIT and for turbulent channel flow at $Re_\tau = 395$ very satisfying results were obtained compared to similar results in the literature using the standard Smagorinsky model (with van Driest damping) and the SA-DES model [34], which can be implemented easily into an unstructured flow solver. A calibration of the model parameters, performed here using least-squares cost functionals for first and second order flow statistics, was done after discretisation error in space and time was ensured to be sufficiently small. The optimized values for the model constant are in close agreement with the values found in literature.

Concerning the *second question* posed in the introduction, turbulent channel flow at $Re_\tau = 4800$ was considered. Wall-functions allow to use larger time step size by factor four and increased spacing in streamwise and spanwise direction by factor five. The savings in wall-normal direction are at least by a factor of four. Based on these numbers, the total savings are thus by a factor of 400. Then turbulent flow over a backward facing step at higher Reynolds number $Re_h = 37500$ by [11] was simulated successfully using wall-functions. It is worth highlighting that the total simulation time using sufficiently fine mesh and time step size is about six days on a single processor machine. This demonstrates the industrial feasibility for engineering design studies for configurations of moderate complexity and relatively large Reynolds numbers.
The *third* and *fourth question* posed in the introduction concern reliability of LES results in terms of numerical error and best-practice guidelines. Convergence studies for turbulent channel flow and backward-facing step showed that the numerical discretisation error in space and time has a dominant influence on the solution and that underresolution can cause poor results. From an industrial view point, the danger of an underresolved LES is judged to be the major hurdle for LES in complex geometries, since it is well-known practice in industry to prefer increasing the complexity of the CAD model rather than to refine the mesh and keep geometrical details constant. The large influence of the spatial discretisation error on the quality of the LES results strongly demands best practice guidelines for mesh design. For LES with near-wall resolution and wall-modelling using wall functions, mesh requirements inside attached boundary layers in streamwise, spanwise and wall-normal direction found in this work confirmed existing best practice guidelines for mesh design. For free-shear layers and regions of separated flow these guidelines cannot be applied. As a remedy, we presented a sensor based on the resolved turbulent kinetic energy which measures the resolution quality of the LES in such flow regions. The sensor values can then be used to refine the mesh locally, e.g. using the techniques in [4]. This will be subject to future research since it would raise a new important question concerning LES on unstructured meshes. Since the present refinement strategy does not support hanging nodes, the refinement of hexaedral elements leads to prismatic and tetraedral elements. The numerical properties of the present method for LES has not yet been studied on such elements. This needs to be done before applying a local mesh refinement.
For LES of flows in complex geometries, grid convergence can generally not be ensured by a global mesh refinement study due to extremely large computational costs. The question whether or not the number of degrees of freedom, which is necessary to achieve mesh converged results for LES, can be reduced by using higher order methods, is beyond the scope of this paper. In any case, the proposed approach of a local grid refinement using a measure for LES resolution quality offers a promising tool to automatically design a mesh such that the LES solution is sufficiently converged for engineering design problems using a low-order code at affordable computational costs.

Acknowledgements

The authors are grateful to Dr. M. Klein for providing the fortran routines for the method [19]. This work benefited immeasurably from the discussions of the first author within the DESider project (Detached Eddy Simulation for Industrial Aerodynamics) a collaboration between ALA, CFX, DASSAV, EADS-M, ECD, LML, NLR, EDF, NUMECA, DLR, FOI, IMFT, ONERA, Chalmers University, Imperial College, TU Berlin, UMIST and NTS. The project is funded by the European Union and administrated by the CEC, Research Directorate-General, Growth Programme, under Contract No. AST3-CT-2003-502842. Special thanks are to Drs. Matthias Orlt, Keith Weinman, Charles Mockett, and Dieter Schwamborn. The second author gratefully acknowledges financial support by the GK 1023 by the Deutsche Forschungsgemeinschaft (DFG). Finally the valuable suggestions by the reviewers are gratefully acknowledged.

References

[1] Guide for the Verification of Computational Fluid Dynamics Simulations. Tech. rep., AIAA G-077-1998 (1998)

[2] A selection of test cases for the validation of large-eddy simulations of turbulent flows (quelques cas d'essai pour la validation de la simulation des gros tourbillons dans les écoulements turbulents. Tech. rep., AGARD-AR-345 (1998)

[3] Aider, J.L., Danet, A., Lesieur, M.: Large-eddy simulation applied to study the influence of upstream conditions on the time-dependant and averaged characteristics of a backward-facing step flow. Journal of Turbulence **8**, DOI: 10.1080/14685240701701,000 (2007)

[4] Alrutz, T., Orlt, M.: Parallel dynamic grid refinement for industrial applications. In: Proceedings of the European Conference on Computational Fluid Dynamics (ECCOMAS CFD 2006) (2006)

[5] Bazilevs, Y., Calo, V., Cottrell, J., Hughes, T., Reali, A., Scovazzi, G.: Variational multiscale residual-based turbulence modeling for large eddy simulation of incompressible flows. Computer Methods in Applied Mechanics and Engineering **197(1-4)**, 173–201 (2007)

[6] Becker, R., Braack, M., Vexler, B.: Parameter identification for chemical models in combustion problems. Applied Numerical Mathematics **54(3-4)**, 519–536 (2005)

[7] Benhamadouche, S., Jarrin, N., Addad, Y., Laurence, D.: Synthetic turbulent inflow conditions based on a vortex method for large-eddy simulation. Progress in Computational Fluid Dynamics **6**, 50–57 (2006)

[8] Choi, H., Moin, P.: Effects of the computational time step on numerical solutions of turbulent flow. Journal of Computational Physics **113**, 1–4 (1994)

[9] Chow, F.K., Moin, P.: A further study of numerical errors in large-eddy simulations. Journal of Computational Physics **184**, 366–380 (2003)

[10] Comte-Bellot, G., Corrsin, S.: Simple eulerian time correlation of full- and narrow-band velocity signals in grid-generated, 'isotropic' turbulence. Journal of Fluid Mechanics **48(2)**, 273–337 (1971)

[11] Driver, D.M., Seegmiller, H.L.: Features of a reattaching turbulent shear layer in divergent channel flow. AIAA Journal **23**, 163–171 (1985)

[12] Faure, S., Laminie, J., Temam, R.: Collocated finite volume schemes for fluid flows Communications in Computational Physics **4**, 1–25 (2008)

[13] Ferziger, J.H., Peric, M.: Computational Methods for Fluid Dynamics. Springer-Verlag, Heidelberg (1996)

[14] Ghosal, S.: An analysis of numerical errors in large-eddy simulations of turbulence. Journal of Computational Physics **125**, 187–206 (1996)

[15] Haase, W., Braza, M., Laurence, D. (eds.): DESider - Detached eddy simulation for industrial aerodynamics. Results of the European-Union funded project, 2004 - 2007. Notes on Numerical Fluid Mechanics and Multidisciplinary Design. Springer, Berlin (to appear)

[16] Johansson, H., Runesson, K., Larsson, F.: Parameter identification with sensitivity assessment and error computation. GAMM-Mitteilungen **30(2)**, 430–457 (2007)

[17] Jovic, S., Driver, D.: Backward-facing step measurements at low reynolds number. Tech. rep., NASA TM 108807 (1994)

[18] Keating, A., Piomelli, U.: A dynamic stochastic forcing method as a wall-layer model for large-eddy simulation. Journal of Turbulence **7**, 1–24 (2006)

[19] Klein, M., Sadiki, A., Janicka, J.: A digital filter based generation of inflow data for spatially developing direct numerical or large eddy simulations. Journal of Computational Physics **186**, 1652–1665 (2003)

[20] Kravchenko, A.G., Moin, P.: On the effect of numerical errors in large eddy simulations of turbulent flows. Journal of Computational Physics **131**, 310–322 (1997)

[21] Le, H., Moin, P., Kim, J.: Direct numerical simulation of turbulent flow over a backward-facing step. Journal of Fluid Mechanics **330**, 349–374 (1997)

[22] Mahesh, K., Constantinescu, G., Moin, P.: A numerical method for large-eddy simulation in complex geometries. Journal of Computational Physics **197**, 215–240 (2004)

[23] Moin, P.: Advances in large eddy simulation methodology for complex flows. International Journal of Heat and Fluid Flow **23**, 710–720 (2002)

[24] Morinishi, Y., Vasilyev, D.: A recommended modification to the dynamic two-parameter mixed subgrid scale model for large eddy simulation of wall bounded turbulent flow. Physics of Fluids **13**, 3400–3410 (2001)

[25] Moser, R.D., Kim, J., Mansour, N.N.: Direct numerical simulation of turbulent channel flow up to $Re_\tau = 590$. Physics of Fluids **11**, 943–946 (1999)

[26] Nikitin, N.V., Nicoud, F., Wasistho, B., Squires, K.D., Spalart, P.R.: An approach to wall modeling in large-eddy simulation. Physics of Fluids **12(7)**, 1629–1632 (2000)

[27] Park, N., Mahesh, K.: Analysis of numerical errors in large eddy simulation using statistical closure theory. Journal of Computational Physics **222**, 194–216 (2007)

[28] Pope, S.B.: Turbulent flows. Cambridge University Press, Cambridge (2000)

[29] Pope, S.B.: Ten questions concerning the large-eddy simulation of turbulent flows New Journal of Physics **6**, 1–24 (2004)

[30] Rhie, C.M., Chow, W.L.: Numerical study of the turbulent flow past an airfoil with trailing edge separation. AIAA Journal **21**, 1525–1532 (1983)

[31] Sagaut, P.: Large eddy simulation for incompressible flows. Springer-Verlag, Berlin (2001)

[32] Spalart, P.R.: Direct simulation of a turbulent boundary layer up to $\mathrm{R}_\theta = 1410$. Journal of Fluid Mechanics **187**, 61–98 (1988)

[33] Spalart, P.R.: Young-person's guide to detached-eddy simulation grids. Tech. rep., NASA/CR-2001-211032 (2001)

[34] Spalart, P.R., Jou, W.H., Strelets, M., Allmaras, S.R.: Comments on the feasibility of les for wings, and on a hybrid rans/les approach. First AFOSR International Conference on DNS/LES, Ruston, LA, 4-8, August, 1997, in: Advances in DNS/LES, edited by C. Liu and Z. Liu (Greyden, Columbus, OH, 1997) (1997)

[35] Templeton, J.A., Wang, M., Moin, P.: An efficient wall model for large-eddy simulation based on optimal control theory. Physics of Fluids (2006). DOI 10.1063/1.2166457

[36] Tessicini, F., Temmerman, L., Leschziner, M.: Approximate near-wall treatments based on zonal and hybrid RANS-LES methods for LES at high Reynolds numbers. International Journal of Heat and Fluid Flow **27**, 789–799 (2006)

[37] Wang, M., Moin, P.: Dynamic wall modeling for large-eddy simulation of complex turbulent flows. Physics of Fluids **14**, 2043–2051 (2002)

[38] Zhang, X.Q.: Identification of model and grid parameters for incompressible turbulent flows. Ph.D. thesis, University Göttingen (2007)